Advanced Composite Materials
Publication details, including instructions for authors and subscription information:
http://www.tandfonline.com/loi/tacm20

Damage suppression in CFRP laminates using embedded shape memory alloy foils

Toshimichi Ogisu , Masakazu Shimanuki , Satoshi Kiyoshima , Junji Takaki & Nobuo Takeda

Version of record first published: 02 Apr 2012.

To cite this article: Toshimichi Ogisu , Masakazu Shimanuki , Satoshi Kiyoshima , Junji Takaki & Nobuo Takeda (2004): Damage suppression in CFRP laminates using embedded shape memory alloy foils, Advanced Composite Materials, 13:1, 27-42

To link to this article: http://dx.doi.org/10.1163/1568551041408778

Adv. Composite Mater., Vol. 13, No. 1, pp. 27–42 (2004)

Also available online - www.vsppub.com

Damage suppression in CFRP laminates using embedded shape memory alloy foils

TOSHIMICHI OGISU [1,*], MASAKAZU SHIMANUKI [1], SATOSHI KIYOSHIMA [1], JUNJI TAKAKI [2] and NOBUO TAKEDA [3]

[1] *Fuji Heavy Industries Ltd., 1-1-11 Yonan, Utsunomiya-city, Tochigi, 320-8564, Japan*
[2] *Innovation Center for Research and Engineering Education, Utsunomiya University, 7-1-2 Yoto, Utsunomiya-city, Tochigi, 321-8585, Japan*
[3] *Graduate School of Frontier Sciences, The University of Tokyo, 7-3-1 Hongo, Bunkyo-ku, Tokyo 113-0033, Japan*

Received 18 July 2003; accepted 3 March 2004

Abstract—This paper presents an overview of the damage growth suppression effects in CFRP laminates using embedded SMA foils, and was conducted to technically verify the application to aircraft structures. In previous studies, the authors confirmed the damage growth suppression of CFRP laminates with embedded pre-strained shape memory alloy (SMA) foils through both coupon testing and structural element testing. Through detailed observation of the damage behavior, we determined that these effects occurred due to the suppression of the strain energy release rate based on the suppression of the crack opening displacement caused by the recovery stress of SMA foils. These results were verified in this study using a demonstrator test article, which was a 1/3-scaled model of a commercial airliner's fuselage structure (B737 class). To demonstrate the damage growth suppression, the lower panel, which was dominated by tension load, was selected as the evaluation area. The evaluation area was an integrated panel including both the 'smart area' (CFRP laminate with embedded pre-strained SMA foils), and the 'conventional area' (standard CFRP laminate), for direct comparison of the damage behavior. The demonstration was conducted at 80°C in the smart area, and room temperature (RT) in the conventional area using a quasi-static load-unload test method. The demonstrator test article identified that the damage onset strain in the smart area was improved by 30% over that in the conventional area.

Keywords: Carbon fiber reinforced plastic (CFRP); shape memory alloy (SMA); damage suppression behavior; recovery stress of SMA; crack opening displacement; strain energy release rate; aircraft; fuselage structure; demonstrator.

*To whom correspondence should be addressed. E-mail: Ogisut@uae.subaru-fhi.co.jp

1. INTRODUCTION

It has been 20 years since the research of smart material and structural systems was introduced. However, most of the research has not yet reached the application stage, although there are some preliminary applications in civil infrastructure fields [1].

Significant needs have been discussed in Europe with respect to the application of the health monitoring system for aircraft structures. A concept design change from a no-damage growth concept to a damage-tolerant concept is expected with the improvement of damage detection capability using the health-monitoring system. This concept change will achieve a drastic weight reduction and ensure high reliability of future airframes [2]. Similar studies are underway in the US also [3]. However, the US focuses mainly on damage-control systems and multifunctional systems for application study. Moreover, actuator materials for system applications were developed in the CHAP program funded by the Defense Advanced Research Projects Agency (DARPA) [4]. Recently, DARPA has been conducting demonstrations of smart material and structural systems with Northrop Grumman [5] and Boeing [6] using an Unmanned Combat Air Vehicle (UCAV) with a variable shape wing of a 30% scale model and an F-15 engine inlet with embedded actuator materials. NASA has started the Morphing Project, which seeks to develop aircraft with embedded multifunctional smart materials such as shape memory alloy (SMA) [7]. The needs for actuator materials have thus become more pressing year-by-year.

Our research focuses on damage suppression in CFRP laminates using the recovery stress of the embedded pre-strained SMA foils as an actuator element. These effects have the potential for drastic weight reduction and performance improvement through innovative technology, such as an increase of the structural design allowable in composite materials. The authors were successful in developing a damage-suppression system using CFRP laminates with embedded pre-strained SMA foils, and confirmed the damage growth suppression experimentally and analytically [8–10]. Furthermore, the damage suppression was also verified with structural element specimens [11]. Damage growth was suppressed by suppressing the strain energy release rate based on suppressing the crack opening displacement [12]. This is done through the recovery stress at the crack tip of the transverse crack generated in the 90-degree ply of the laminates. In the present study, a technical verification test was conducted to demonstrate damage growth suppression using a demonstrator test article.

2. DEMONSTRATOR

2.1. Concept

The demonstrator test article is designed as a 1/3-scale model of a commercial airliner's fuselage structure (B737 class), which is the integrated test article in the Japanese national project on 'Smart materials and structural systems'. For aircraft

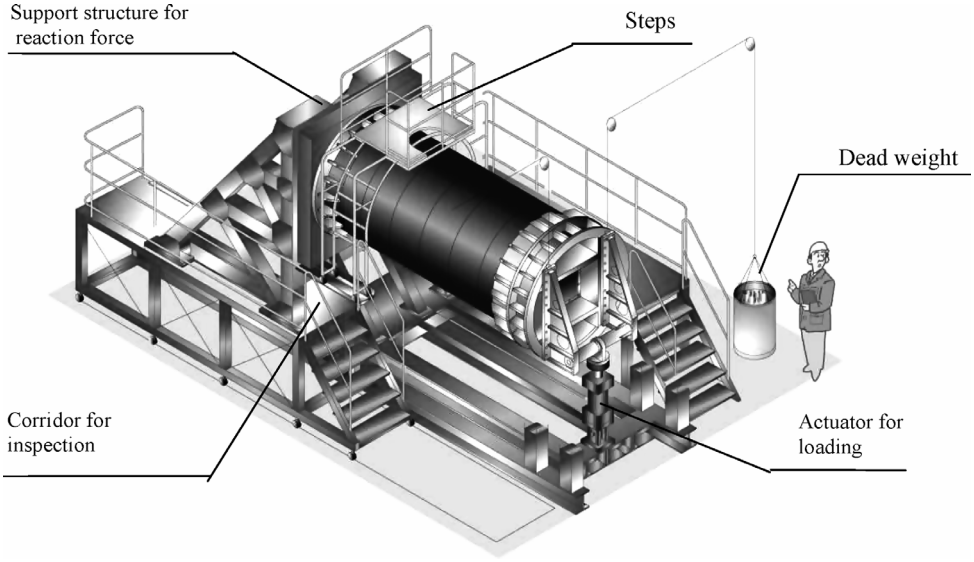

Figure 1. Schematic of demonstrator test set-up.

design, material properties must be certified at several development test stages, such as coupon, structural element, subscale test and actual structure. At each test phase, several parameters should be considered, such as the size effect, manufacturability, fixture design, and assembly method. These test approaches for aircraft design and manufacturing are defined as the 'Building Block Approach' in accordance with MIL-HANDBOOK-17 [13]. In aircraft design, it is important that coupon test data of the material be used up to the actual structure design through all the test phases. The present demonstrator test is a subscale test and is very important for certifying the strength, manufacturability, and assembly of the subscale structure. In this study, the demonstrator was designed and manufactured to technically verify damage detection and the damage growth suppression. Figure 1 outlines the schematic concept of the demonstrator test set-up.

2.2. Technical verification in demonstrator

The authors developed a damage suppression system using CFRP laminates with embedded pre-strained SMA foils in a previous study. The system effectiveness was confirmed through both coupon tests and structural element tests. In the demonstrator test article, the damage suppression effect using embedded pre-strained SMA foils in CFRP laminates was confirmed with regard to the following theme, objectives, and verification methods.

Demonstration theme	Develop a damage-suppression system using embedded pre-strained SMA foils for the composite fuselage demonstrator.
Purpose	Technically verify the damage onset and growth-suppression by the embedded pre-strained SMA foils in CFRP laminates.
Verification methods	Set up the integrated panel including both CFRP laminates only (conventional area) and CFRP laminates with embedded pre-strained SMA (smart area) as the lower panel of the demonstrator. Compare the damage onset and growth behavior of the two areas directly at the edge surface of a 1-inch hole in the evaluation area using the penetrant inspection method.

2.3. Design of the demonstrator's lower panel

Figure 2 depicts the assembly configuration of the demonstrator's lower panel. The lower panel consists of 1/4 of the whole demonstrator of 1.5 m in diameter and 3 m in length. The specification of the structure is 200 mm in stringer pitch, and 500 mm in frame pitch like general skin-stringer structures. The composite blade-type stringers were bonded to the composite skin structure.

The lower panel was divided lengthwise into three parts. The center panel between STA1500 and STA2500 is the evaluation area. The lower panel was assembled by fastening the frame (aluminum alloy), support fitting (steel) and loading fitting

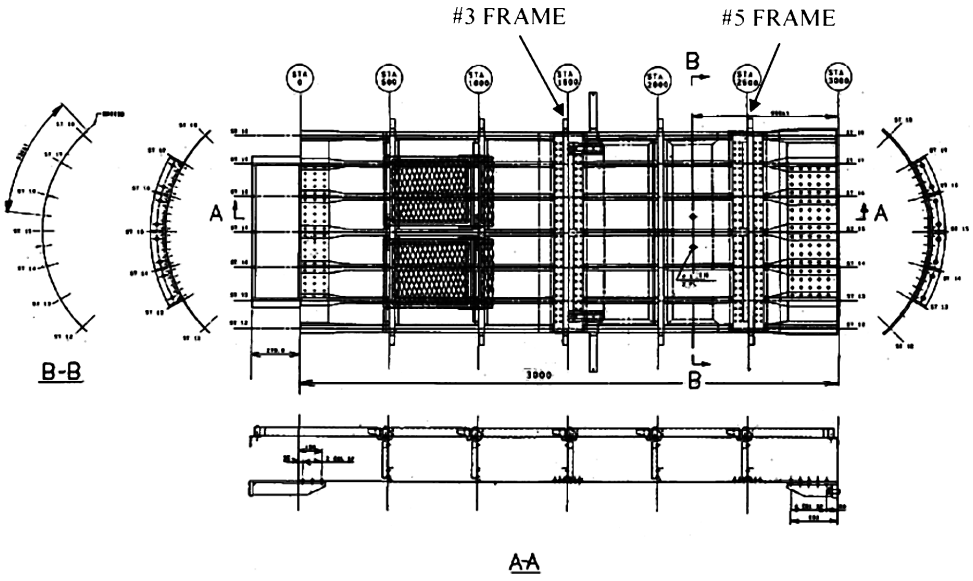

Figure 2. Assembly configuration of lower panel.

(steel) at both edges. The #3 (STA1500) and #5 (STA2500) frames and the lower skin were fastened with the inserted splice plate (aluminum alloy) to connect the lower skin longitudinally. The assembly with the side panel was fastened with an outer flange of the protruding frame from inside of the lower panel; both the lower and side frames were fastened at the same time. When the CFRP structures contacted aluminum alloy, glass fabric was applied to the contact area.

2.4. Evaluation area

The goal of this demonstrator program is to verify how embedded, pre-strained SMA in CFRP laminates suppress damage from and growth of transverse cracks and delamination initiating from the transverse cracks when a CFRP laminated structure is subjected to cyclic loads. Tension loads easily generate transverse cracks in CFRP laminates in 90-degree plies. Therefore, the lower side of the demonstrator that is in tension was selected as the evaluation area. Figure 3 displays some details of the evaluation area in the lower panel. The evaluation area is an integrated panel including both CFRP laminates only and CFRP laminates with embedded pre-strained SMA foils areas for direct comparison. Both the standard and smart areas in the integrated panel were subjected to the same strain level. Therefore, an increase in the crack onset strain of the CFRP laminate with embedded pre-strained SMA foils compared with standard CFRP laminates will verify that damage was suppressed. Areas are defined as a conventional area or a smart area. A 1-inch (25.4 mm) hole was drilled in each area to simulate an access hole and an antenna hole. The damage suppression was evaluated by observing the damage at the edge of the hole. The CFRP laminate with embedded pre-strained SMA

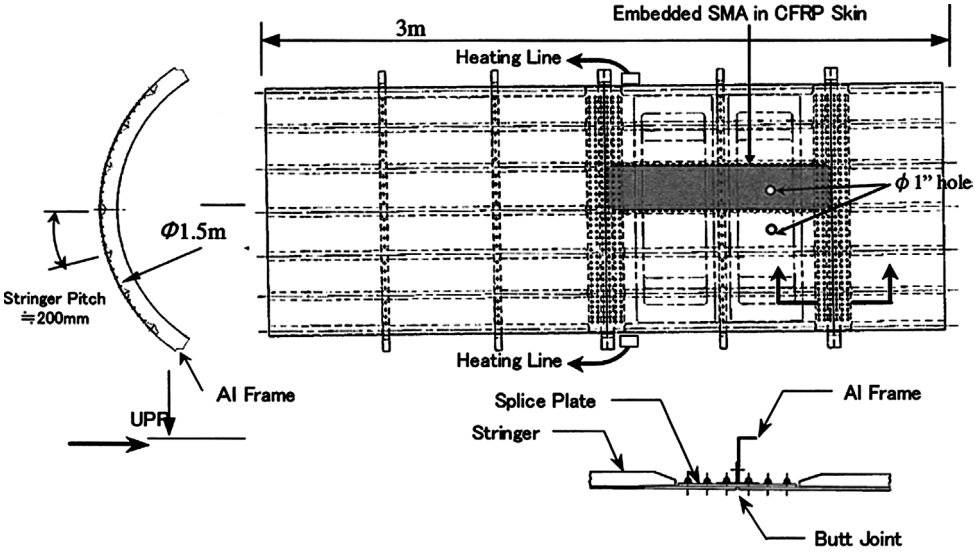

Figure 3. Evaluation area of lower panel.

foils suppressed damage through the relaxation of thermal residual stress in the 90° ply of the laminate and the suppression of the strain energy release rate due to the relaxation of local stress concentration. The suppression of the strain energy release

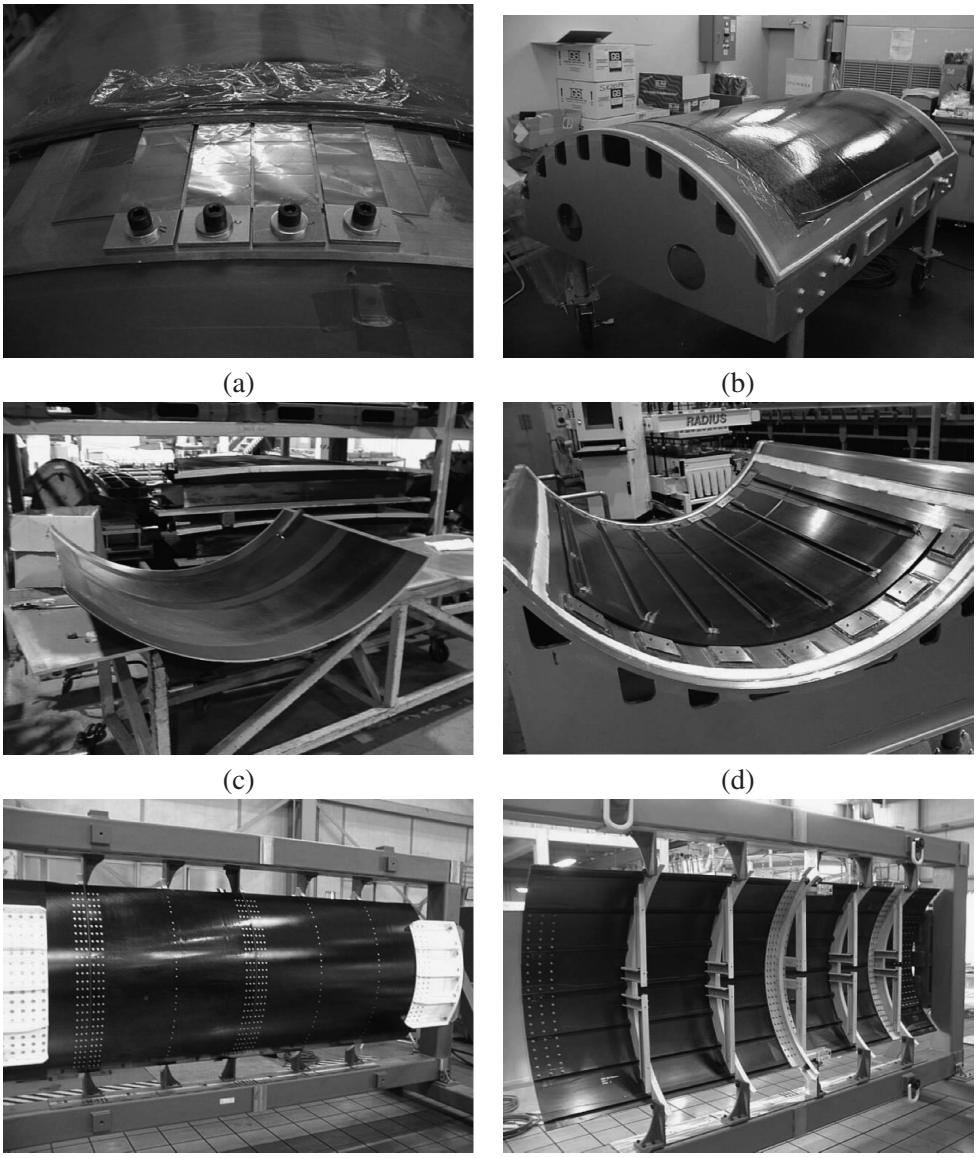

Figure 4. Manufacturing overview of the demonstrator (a) Restraining jig and SMA, (b) Lay-up of the panel, (c) After curing of the panel, (d) Post-cured stiffened panel, (e) Outside view of the lower panel, (f) Inside view of the lower panel.

rate is related to the decrease in crack opening displacement, which leads to the decrease in crack multiplication and delamination.

3. MANUFACTURING OF LOWER PANEL OF DEMONSTRATOR

3.1. Materials

This study used Ti-Ni SMA foils (Furukawa Electric Co., Ltd.; thickness 0.04 mm). The prepreg system used was T300/F593 (thickness 0.2 mm), which is a unidirectional prepreg system of the medium stiffness carbon fiber and epoxy resin (Hexcel Corp.; 350° F cured). Epoxy adhesive films (Metlbond 1515-3, Cytec Industries; thickness 0.125 mm) were used to increase the bonding between CFRP and SMA foils.

3.2. Manufacturing demonstrator

The evaluation area consists of an integrated panel including both a conventional area ([+45/0/−45/90]s) and a smart area ([+45/0/−45/90/Ad/2% Pre-Strained SMA/Ad/90/−45/0/45], Ad: film adhesion ($t = 0.125$ mm)). The nominal thickness is 1.6 mm in the conventional area and 1.89 mm in the smart area. SMA foils were cleaned and roughened by 3% fluoride acid–15% nitric acid to remove the oxide film created when the material was mechanically rolled. The SMA foils were anodic-oxide treated with 10% NaOH solution [8]. The SMA foils were cleaned by solvent when the laminates were manufactured. The laminates were manufactured using a special fixture that was able to restrain the pre-strain of SMA foils. Figure 4 presents a view of the demonstrator being manufactured.

4. DEMONSTRATOR TEST RESULTS

4.1. Test procedure

Figure 5 depicts the set-up of the demonstrator test article. The demonstrator test was conducted using the cyclic loading method by applying an upward bending load to the fuselage structure using two actuators. The lower panel was therefore primarily subjected to tension loads. The torsion was controlled by confirming the load balance of the two actuators attached to the loading fixture and by confirming the strain balance between the conventional area and the smart area.

Figure 6 presents the demonstrator load history. In phase 1, the demonstrator was tested under load control condition using the calibrated stress–strain relationship obtained by strain survey up to $3600\mu\varepsilon$ (maximum predicted load 22 tonf or 215 600 N). The arrows represent the damage observation interval at the edge of holes in the evaluation area. The demonstrator test was conducted in increments of $250\mu\varepsilon$ steps to $3000\mu\varepsilon$ and $200\mu\varepsilon$ steps to $4000\mu\varepsilon$. The demonstrator test

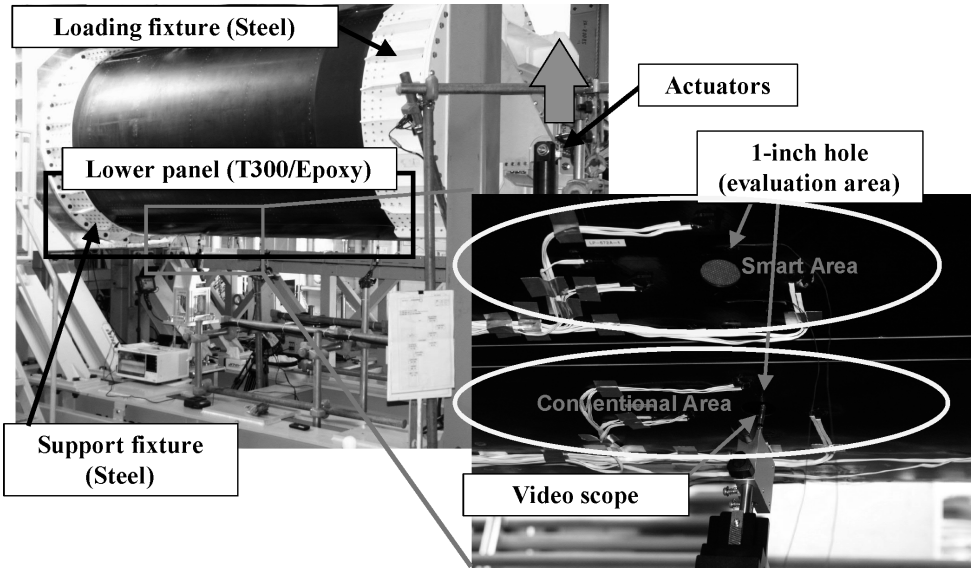

Figure 5. Set-up of demonstrator test article.

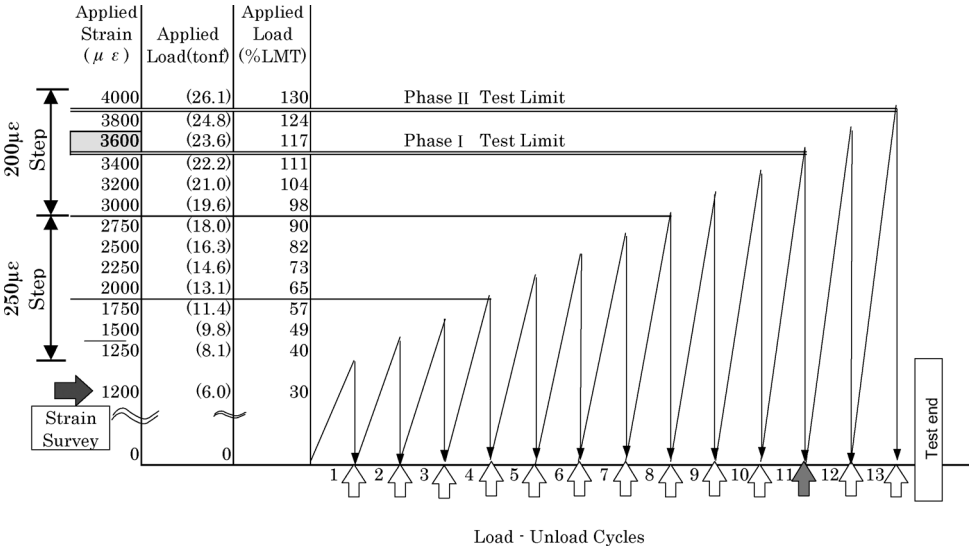

Figure 6. Load history of demonstrator.

was divided into two phases, phase I to 3600μ and phase II to 4000μ from the relationship of the fracture probability and the feasibility of the technical verification. The applied strain was controlled by the load control. The output strain of the first cycle started from a loading of 1250$\mu\varepsilon$. After that, the damage observations were made at each strain step.

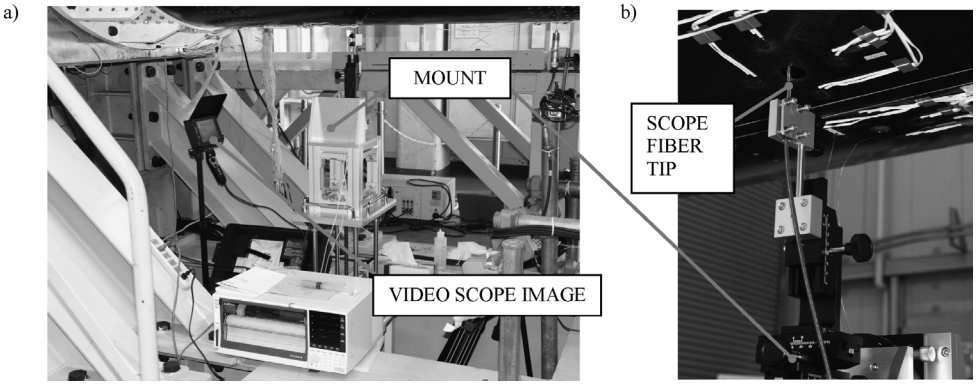

Figure 7. Set-up of damage observation system.

4.2. Damage observation method

Figure 7 illustrates the set-up of the damage observation system for the demonstrator. A video scope system (Olympus Industries; Iplex; 5 mm fiber diameter) was used to observe the edges of 1-inch holes drilled in the evaluation area of the lower panel. The system can observe damage and perform digital recording. The scope was fixed with a special fixture mount that could transition up and down, right and left, front and back, and rotate around three axes to observe the evaluation area (including the smart area and the conventional area). The observation was conducted in the smart area and conventional area in each loading cycle, as demonstrated in Fig. 6.

4.3. Location of strain gages and thermocouples

Figure 8 illustrates the location of strain gages (G-1 to G-8) and thermocouples (T/C-1 and T/C-2) in the lower panel of the demonstrator. Strain gages were glued to the outer side of the demonstrator. The thermocouples were attached to the outer side of the demonstrator by CAPTON tape. The strains in the longitudinal direction (G-1, 4 (smart area) and G-5, 8 (conventional area) gages) were used for load control of the actuator. The location of the strain gages did not affect the strain distribution in the structural element test.

4.4. Current heating

Current heating was used in the demonstrator test article to provide the recovery stress for the SMA foil. A previous study confirmed that the recovery stress was generated by current heating [9]. Therefore, a current-heating system was integrated into the demonstrator test article. Figure 9 depicts the current-heating terminals. The SMA foils were connected by a micro-spot welding method. The fastening bolts in the area with SMA foils embedded were coated by ceramics to prevent electrical leakage. Uniform heating was achieved by applying the current-heating system to the structural element specimen, as shown in Fig. 10.

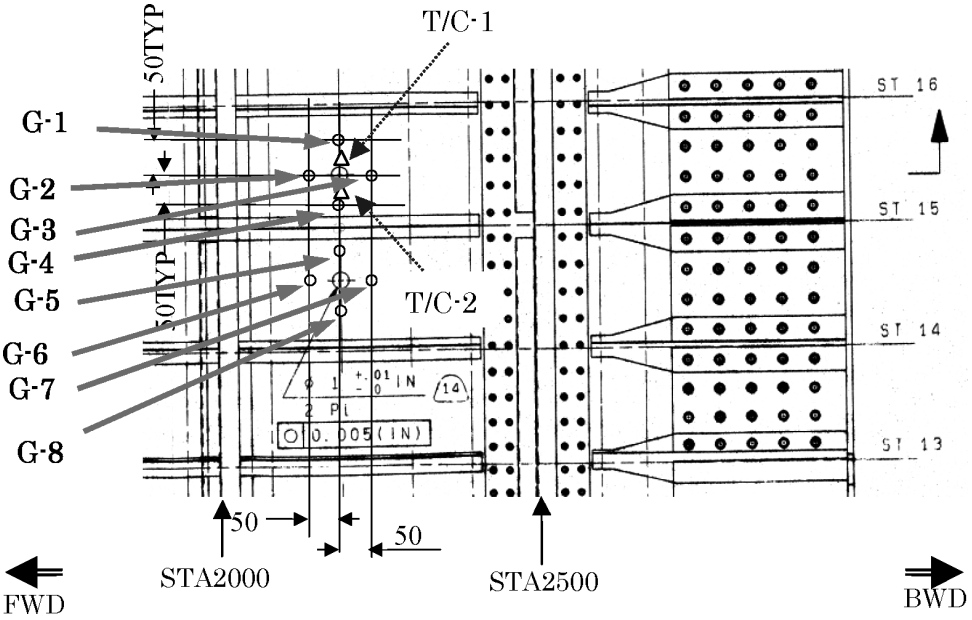

Figure 8. Gage location of the evaluation area (a view from inside).

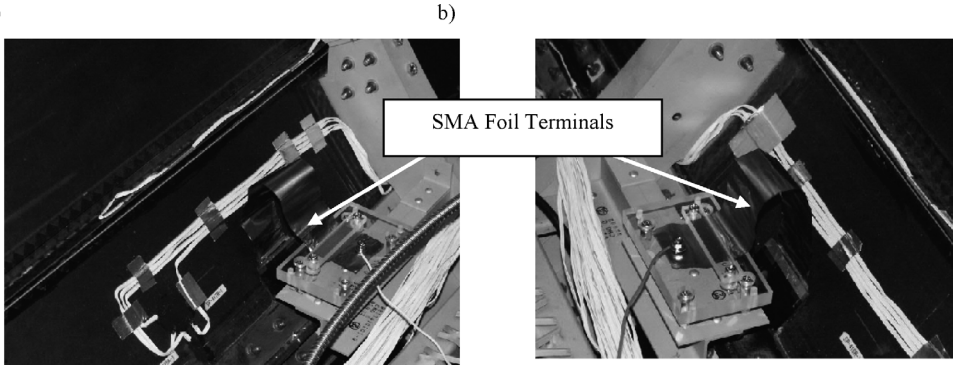

Figure 9. Current heating system of SMA foils.

Some over-heating in the demonstrator was observed in local areas at the connecting points of SMA foils. SMA foils were therefore heated by both current heating and a silicon rubber heater. Figure 11 illustrates the set-up of the silicon rubber heater.

4.5. Results

Figure 12 displays the applied loads and applied strains as a function of the testing time up to the loading of 3600$\mu\varepsilon$. 'FL' represents an applied load on the left-hand side of the demonstrator as viewed from the support fitting; the 'FR' represents an applied load on the right-hand side at the same distance. G-1L, G-4L, G-5L and

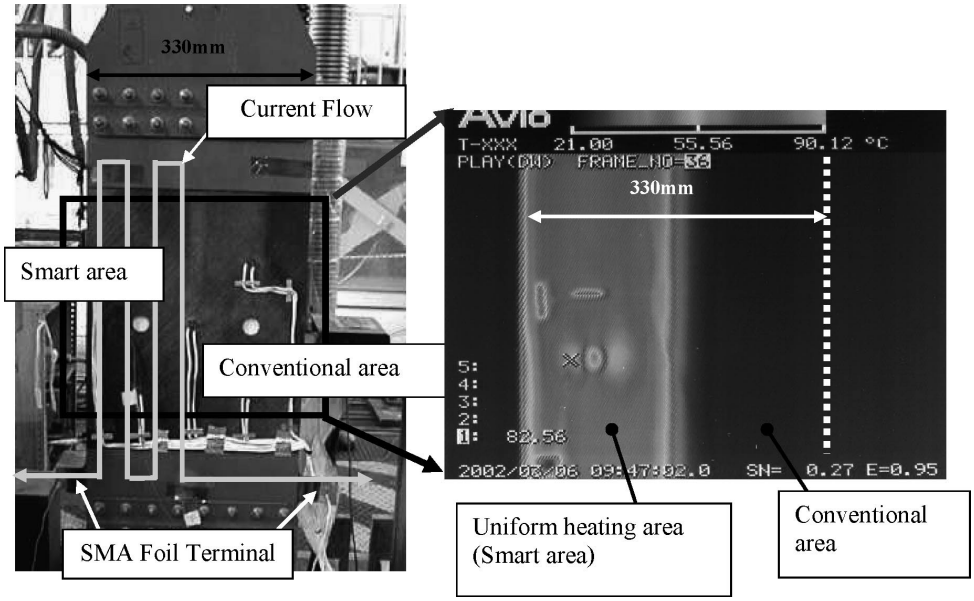

Figure 10. Current heating in the structural element test.

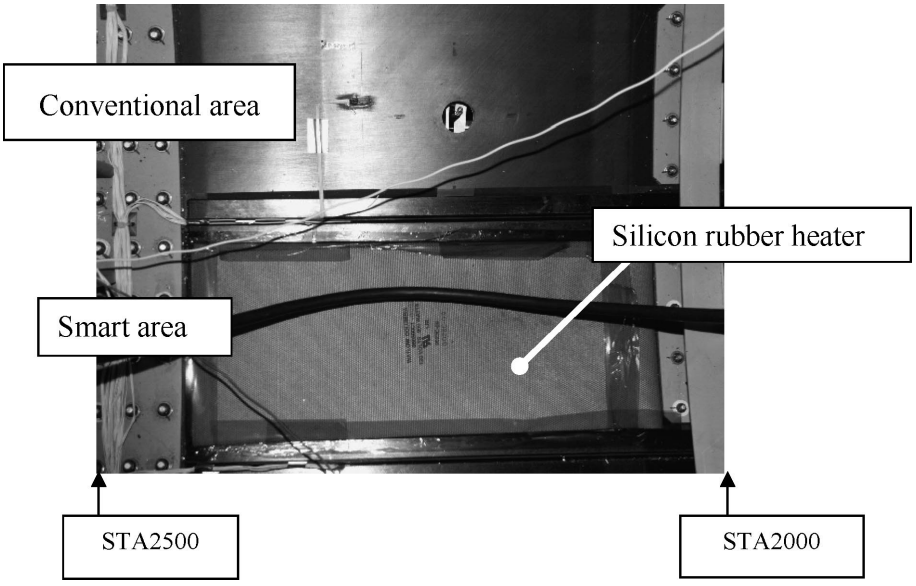

Figure 11. Set-up view of silicon rubber heater on the smart area.

G-8L represent applied strains in the longitudinal direction. As results indicate, the applied load exhibited good balance under the control of two actuators. The strains of both the smart and conventional areas were confirmed to exhibit the same strain level for the same load. Figure 13 depicts transverse crack onset at both 2500$\mu\varepsilon$

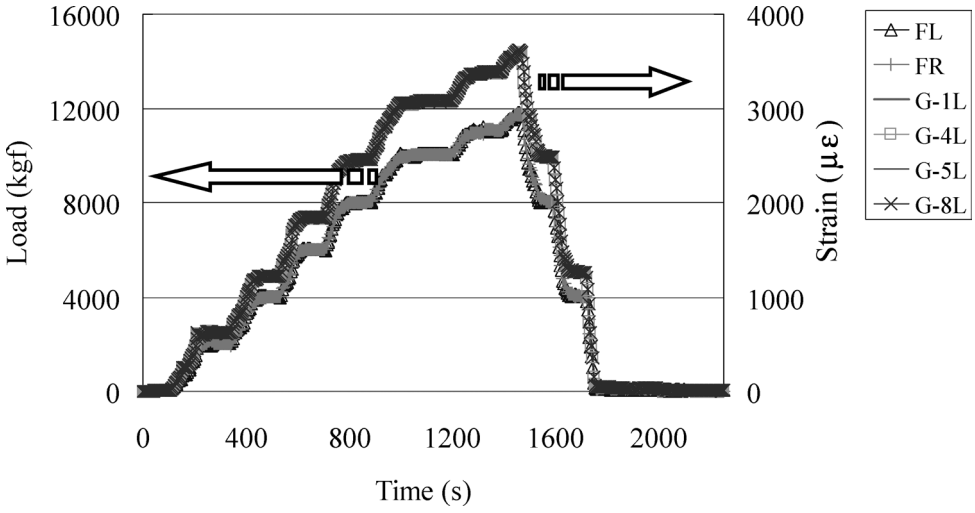

Figure 12. Load–strain curves as a function of the testing time up to $3600\mu\varepsilon$.

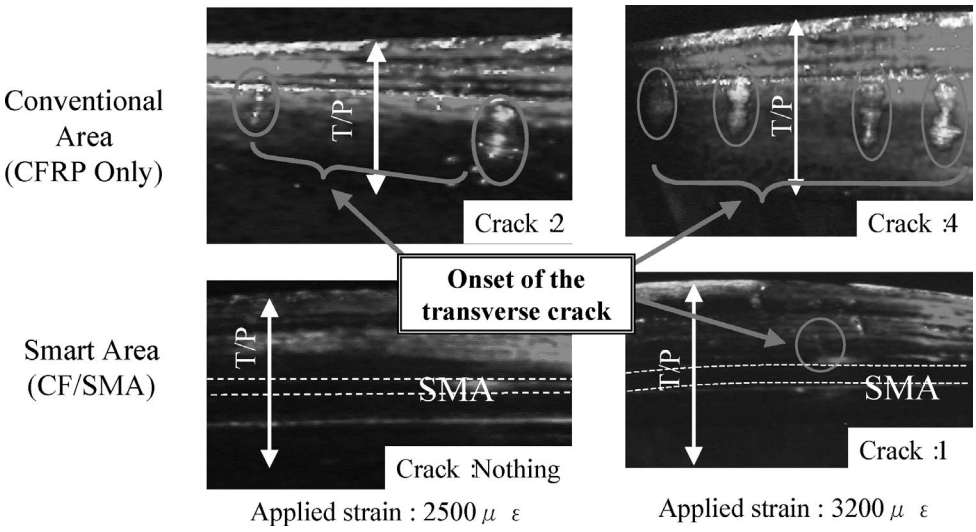

Figure 13. Observation of the transverse crack onset strain in the demonstrator.

and $3200\mu\varepsilon$; Fig. 14 depicts delamination onset at $3800\mu\varepsilon$. Table 1 summarizes the demonstration test. As shown in Fig. 13, the first transverse crack was observed at $2500\mu\varepsilon$ in the 90-degree ply of the conventional area, but no transverse crack was observed in the smart area at this strain level. Therefore, the applied strain was increased. At an applied strain of $3200\mu\varepsilon$, the first transverse crack was observed in the smart area, while the transverse crack density in the conventional area at that strain level had doubled. The demonstrator test results confirmed that the damage onset strain increased and that crack multiplication was suppressed.

Table 1.
Summary of demonstration test

SEG No.	Load %LMT	Norminal strain of evaluation area ($\mu\varepsilon$)	Load of smart area (kgf) [N]	Load of conventional area(kgf)	Strain gage G-1L (smart) ($\mu\varepsilon$)	Strain gage G-4L (smart) ($\mu\varepsilon$)	Strain gage G-5L (conventional) ($\mu\varepsilon$)	Strain gage G-8L (conventional) ($\mu\varepsilon$)	Smart 80°C	Conventional RT
1	0%	0	0 [0]	0	0	0	0	0	None	None
2	40%	1250	4030 [39 494]	4100	1261	1254	1252	1253	None	None
3	49%	1500	4898 [48 000]	4929	1504	1508	1512	1510	None	None
4	57%	1750	5709 [55 948]	5739	1737	1742	1752	1759	None	None
5	65%	2000	6532 [64 013]	6530	2013	2009	2011	2003	None	None
6	73%	2250	7268 [71 226]	7378	2251	2253	2251	2250	None	None
7	82%	2500	8161 [79 978]	8150	2489	2487	2501	2507	None	T-Crack Onset : 2
8	90%	2750	8984 [88 043]	8985	2730	2749	2752	2764	None	T-Crack: 2
9	98%	3000	9758 [95 628]	9826	2989	2994	3014	3008	None	T-Crack: 2
10	104%	3200	10 506 [102 959]	10449	3169	3198	3214	3215	T-Crack Onset : 1	T-Crack: 4
11	111%	3400	11 080 [108 584]	11116	3369	3385	3408	3407	T-Crack: 1	T-Crack: 4
12	117%	3600	11 798 [115 624]	11777	3582	3591	3608	3611	T-Crack: 1	T-Crack: 5 T-Crack : 5 Delamination
13	124%	3800	12 540 [122 892]	12466	3795	3793	3812	3817	T-Crack: 2	Onset
14	131%	4 000	13 133 [128 703]	13083	3969	3998	4017	3999	T-Crack: 3	T-Crack: 9

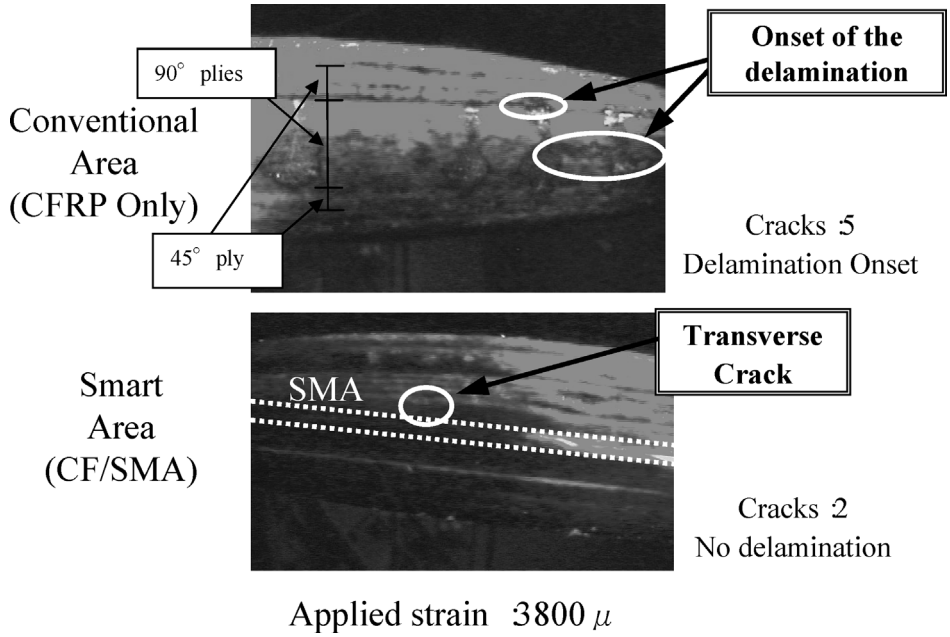

Figure 14. Observation of the delamination onset strain in the demonstrator.

Figure 14 demonstrates that the first delamination was generated at 3800μ at the interface of [−45/90] ply and the intralaminar region of the 90-degree ply in the conventional area. The smart area had no delamination and only two transverse cracks at this high strain level.

The demonstration verified that the damage onset and growth strain in the smart area was improved by 30% over that of the conventional area.

4.6. Discussion

Figure 15 predicts the damage onset strain in the demonstrator using the results of both coupon and structural elements.

Strain levels for transverse cracking, delamination and fracture were predicted as follows based on previous test results.

The design strain tolerance in the evaluation area of the demonstrator was decided from both the coefficient of variation (CV) of the coupon test and the average strain of the structural element test. For example, the fracture probability of the demonstrator was required to be A value (1% fracture at 95% confidence). (Data indicated by an asterisk were derived from the one-side tolerance limit factor, when $n = \infty$ for nominal distribution in accordance with MIL-HANDBOOK-5.)

$$\begin{aligned}\text{Fracture limit strain} &= m - 2.326^* \times \text{C.V.} \times m \\ &= 4462 - 2.326^* \times 0.0402 \times 4462 \\ &= 4046\mu\varepsilon.\end{aligned}$$

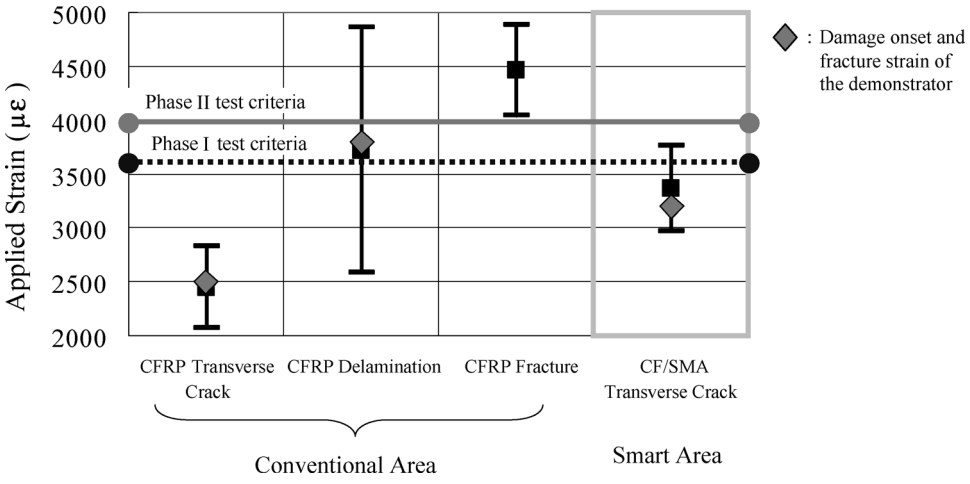

Figure 15. Comparison of the demonstrator test data with the prediction of transverse crack, delamination and fracture strain using the previous test data.

Here, m is the average strain. Predicted onset strains of bar charts can be calculated similarly.

In the demonstrator test Phase I (up to $3600\mu\varepsilon$), transverse cracking occurred in the demonstrator test article at $2500\mu\varepsilon$ in the conventional area and $3200\mu\varepsilon$ in the smart area. These results agreed with the average of transverse cracking that occurred in the structural element test. No delamination occurred in the demonstrator in either the smart area or conventional area in the Phase I test. However, delamination was predicted to be generated at $4000\mu\varepsilon$ in the conventional area in the Phase I test when the average onset strain of coupon and structural element tests and the results of the Phase II test were used. In the actual PhaseI test, delamination occurred at $3800\mu\varepsilon$ as shown in Fig. 15. This means that the coupon and structural element data can be applied as design data for aircraft structures.

Through the demonstration, the damage growth suppression obtained in the coupon test and structural element test was verified in the modeled fuselage structure.

5. CONCLUSION

The demonstrator program has technically verified the damage suppression in CFRP laminates using embedded pre-strained SMA. The successful demonstration of this program suggests the high feasibility of applying the system to aircraft structures.

Acknowledgements

This research was conducted as a part of the 'R&D for Smart Materials and Structures System' project (1998-2002) within the Academic Institutions Centered Pro-

gram supported by NEDO (New Energy and Industrial Technology Development Organization), Japan.

REFERENCES

1. H. Iwaki and N. Takeda, Structural health monitoring system using embedded FBG-based sensors for a damage tolerant building, in: *Proc. 9th SPIE Smart Structures and Materials 2002*, Vol. 4696, pp. 62–73 (2002).
2. H. J. Schmidt and B. Schmidt-Brandecker, Structure design and maintenance benefits from health monitoring systems, in: *Proc. 3rd International Workshop on Structural Health Monitoring: The Demands and Challenges*, Fu-Kuo Chang, pp. 80–101 (2001).
3. C. Fu-Kuo, Ultra-reliable and super-safe structure for the new century, in: *Proc. 1st European Workshop Structural Health Monitoring 2002*, pp. 3–12 (2002).
4. E. Garcia, Smart structures and actuators: past, present, and future, in: *Proc. 9th SPIE Smart Structures and Materials 2002*, Vol. 4698, pp. 1–12 (2002).
5. J. Kudva, B. Sanders, J. Pinkerton-Florance and E. Garcia, The DARPA/AFRL/NASA smart wing program-final overview, in: *Proc. 9th SPIE Smart Structures and Materials 2002*, Vol. 4698, pp. 37–43 (2002).
6. D. M. Pitt, J. P. Dunne and E. V. White, SAMPSON smart inlet design overview and wind tunnel test, Part I: design overview, in: *Proc. 9th SPIE Smart Structures and Materials 2002*, Vol. 4698, pp. 13–23 (2002).
7. A. M. McGowan, A. E. Washburn, L. E. Horta, R. G. Bryant, D. E. Cox, E. J. Siochi, S. L. Padula and N. M. Holloway, Recent results from NASA's morphing project, in: *Proc. 9th SPIE Smart Structures and Materials 2002*, Vol. 4698, pp. 97–111 (2002).
8. T. Ogisu, N. Ando, J. Takaki, T. Okabe and N. Takeda, Improved surface treatment of SMA foils and damage suppression of SMA-foil embedded CFRP laminates, *J. Intelligent Mater. Structure System* **12** (4), 265–270 (2001).
9. T. Ogisu, M. Nomura, N. Ando, J. Takaki, M. Kobayahsi, T. Okabe and N. Takeda, Development of damage suppression system using embedded SMA foil in CRRP laminates, in: *Proc. 8th SPIE Smart Structures and Materials 2001*, Vol. 4333, pp. 387–398 (2001).
10. M. Kobayashi, D.-Y. Song, T. Ogisu and N. Takeda, Mechanical properties of CFRP laminates with embedded SMA foils, in: *Proc. 2nd Asian–Australasian Conference on Composite Materials*, pp. 1065–1070 (2000).
11. T. Ogisu, M. Nomura, N. Ando, J. Takaki and N. Takeda, Application studies of CFRP laminates with embedded SMA foils for aircraft structures, in: *Proc. 9th SPIE Smart Structures and Materials 2002*, Vol. 4698, pp. 343–354 (2002).
12. T. Ogisu, M. Shimanuki, J. Takaki, I. Taketa and N. Takeda, Experimental damage behavior analysis using CFRP laminates with embedded SMA foils under quasi-static uni-axial tension load, in: *Proc. 1st European Workshop Structural Health Monitoring 2002*, pp. 893–899 (2002).
13. MIL-HDBK-5F, *Metallic Materials and Elements for Aerospace Vehicle Structures*, Volume 2 of 2. Guidelines for the Presentation of Data (1990).